ISSN 0031-918X, Physics of Metals and Metallography, 2020, Vol. 121, No. 13, pp. 1301–1308. © Pleiades Publishing, Ltd., 2020.

STRUCTURE, PHASE TRANSFORMATIONS, AND DIFFUSION

Production of NiAl–(Cr,Mo) Eutectic Alloys and Their Cyclic Oxidation Behavior at 800–1000°C

Y. Garip[a], C. Ceper[a], N. Ergin[a], A. S. Demirkıran[b], and O. Ozdemir[a, *]

[a]*Sakarya Applied Science University, Technology Faculty, Department of Metallurgy and Materials Engineering, Esentepe Campus, 54187 Sakarya-Turkey*

[b]*Sakarya University, Engineering Faculty, Department of Metallurgy and Materials Engineering, Esentepe Campus, 54187 Sakarya-Turkey*

**e-mail: oozdemir@sakarya.edu.tr*

Received June 2, 2019; revised March 10, 2020; accepted March 12, 2020

Abstract—Ni–33Al–34Cr and Ni–33Al–28Cr–6Mo (at %) eutectic alloys were produced by the resistive sintering (RS) technique using elemental powders. The cycle oxidation behaviors of alloys at 800, 900, and 1000°C for 168 h in air atmosphere were investigated. The oxidation resistance of alloys was evaluated by the weight change measurements. The activation energy for NiAl–34Cr and NiAl–28Cr–6Mo alloys was 57 and 31 kJ mol^{-1}, respectively. X-ray diffraction (XRD), scanning electron microscopy (SEM), and energy-dispersive spectroscopy (EDS) were performed to characterize the initial microstructure and the oxidation products. The obtained results showed that the oxidation products mainly consist of Cr_2O_3, α-Al_2O_3, NiO, and $NiAl_2O_4$ oxides.

Keywords: NiAl intermetallic, oxidation, alloying element, resistive sintering (RS)

DOI: 10.1134/S0031918X20130062

INTRODUCTION

The NiAl intermetallic compounds have drawn attention as materials for high-temperature applications thanks to their superior properties such as high melting point (1638°C), lower density (≈5.9 g/cm^3), high thermal conductivity (>6 W/m/K), and high corrosion and oxidation resistance at high temperatures [1–3]. However, these materials have low fracture toughness, low plasticity at room temperature, poor creep resistance, and low strength at high temperatures [3]. In order to enhance their strength properties, refractory metals, such as Mo, W, and Ta, are introduced into the NiAl alloys [2]. Bei et al. [4] and Ferrandini et al. [5] reported that after the refractory metal Mo was added to the NiAl alloy the latter acquired superior mechanical properties. It is worth mentioning that among NiAl–(Cr,Mo) eutectic alloys, NiAl–28Cr–6Mo (at %) alloy is considered as one of the most attractive materials because of its unique combination of high fracture toughness at ambient temperature, good ductility, and adequate high-temperature strength [3].

The resistive sintering (RS) technique has attracted attention as a new powder metallurgy approach for producing intermetallics, ceramics, and composite materials. The RS process is regarded as an ever-growing and effective fabricating technology. The most significant property of the RS is that the powder or the green compact is heated by the Joule effect and thus, the materials can be synthesized uniformly and rapidly. As a result, materials with high density and fine microstructure can be to obtain in very short processing time [6–8].

Many investigations have been conducted on the oxidation behavior of NiAl-based alloys [9, 14]. However, little attention has been attracted to the oxidation behavior of NiAl–(Cr,Mo) eutectic alloys. Among many papers related to oxidation [15, 16] only several refer to cyclic oxidation properties of NiAl–(Cr,Mo) alloys. Therefore, evaluation of the cyclic oxidation properties of NiAl–(Cr,Mo) eutectic alloys is of great importance.

EXPERIMENTAL DETAILS

Material Preparation

The eutectic alloys with a nominal composition of Ni–33Al–34Cr and Ni–33Al–28Cr–6Mo (at %) were produced by resistive sintering (RS) technique. The powders contain Ni (99.8%, size 3–7 μm), Al (99.5%, size 10 μm), Cr (99.8%, the particulate size 5 μm), and Mo (99.9%, size 3 μm). According to the nominal composition, all powders weighed by using the electronic balance.

The mechanical mixer was used to obtain a homogenous powder mixture for a period of 5 hours at a rotation speed of 180 rev./min in a dry environment. Then

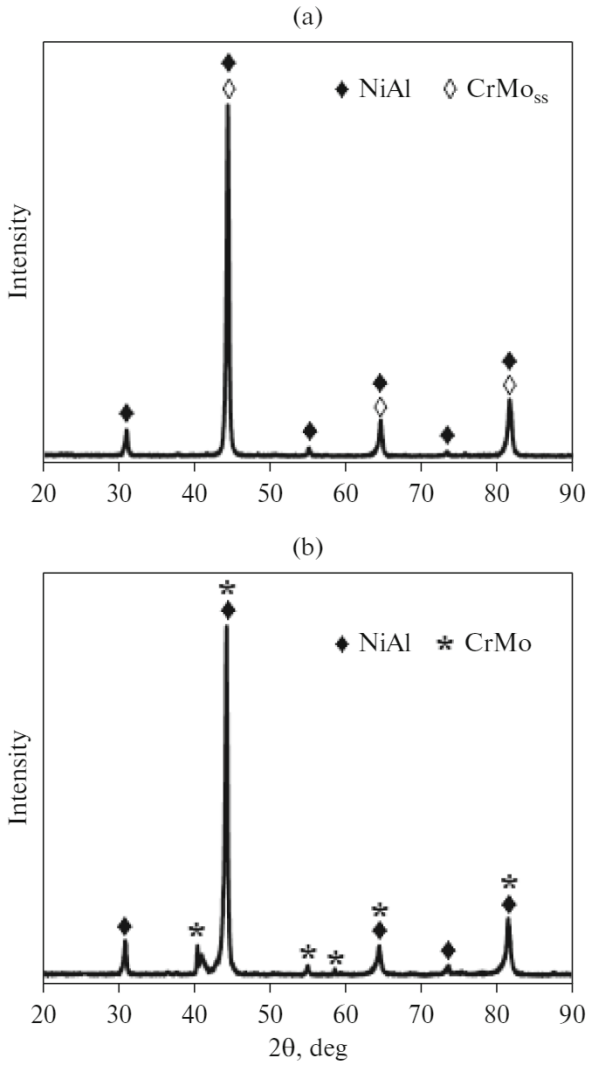

Fig. 1. XRD patterns of (a) NiAl–34Cr, (b) NiAl–28Cr–6Mo alloys produced by RS.

6 g of powder mixture was filled into a steel die with a 20 mm internal diameter. The powder mass was sintered via RS by applying a sintering pressure of 80 MPa at 4200 amperes for 35 minutes in the air. The applied pressure was maintained up to the end of the process. At the completion of sintering, the sintered sample was taken from the die using uniaxial load and was allowed to cool down to ambient temperature.

Cyclic Oxidation Test

Before the hot corrosion test, the original surface area of each samples was at tested using the Solidworks and then weighed by an electronic scale with an accuracy of 0.01 mg. The oxidation tests were conducted in an electric resistance furnace at 800, 900, and 1000°C with 14 cycles up to 168 h. A cycle involves heating the samples to the test temperature and holding them in the furnace for 12 h. At the end of the cycle, the samples were removed from the furnace and then air cooled in/at room temperature. Afterwards, the samples were again weighed to evaluate the oxidation kinetics. This procedure was reapplied for each oxidation cycle.

Characterization

In order to perform the SEM studies, the sintered samples were gradually grounded by SiC papers up to 1200 m and subsequently polished using 1-m dispersion diamond paste. The relative densities of the samples were calculated by Archimedes' principle, based on the immersion technique in distilled water. The microhardness of the samples was determined using Vickers diamond indenter. For both samples, 4 measurements were performed using the application of a 100 g load for a 10 sec. dwell time and then the average of 4 measurements was recorded.

X-ray diffraction analysis (Rigaku, D/MAX-B/2200/PC) was employed to identify the phase constitution of the samples and oxidation products using diffractometer with Cu$K\alpha$ radiation and operated at 40 kV and 40 mA. Data were obtained in result of scanned in the 2θ range from 20° to 90°. The surface morphologies of the oxidation products were characterized by a scanning electron microscope (SEM, JEOL) and microanalysis as carried out by means of an energy dispersive spectroscopy (EDS).

RESULTS AND DISCUSSION

Oxidation Behaviors

XRD analysis of produced NiAl–34Cr and NiAl–28Cr–6Mo (at %) alloys are shown in Fig. 1. According to XRD analysis, the alloys were composed of Cr and NiAl phases. In the NiAl–Cr phase diagram, phase transformation was reported as a result of eutectic reaction (L = A2 + B2) [17].

The chromium-rich disordered A2 solid solution with low NiAl solubility and the NiAl-rich ordered B2 solid solution with low Cr solubility can be seen in the NiAl–Cr phase diagram. From the SEM images in Fig. 2a, it is obvious that the microstructure of the Ni–33Al–34Cr alloy consists of two different phase areas.

The results of EDS analysis in Table 1 show that the area marked as 1 is a Cr rich phase while the one marked as 2 is a NiAl phase with low Cr concentration. The solubility of the chromium element in the NiAl phase is reported to be about wt % 1–5 [18]. Furthermore, the SEM image in Fig. 2a shows that the NiAl phase with a flat surface morphology tends to form Cr phase at the grain boundaries. The presence of Mo-rich white tone phase areas (marked as 4) in the microstructure can be seen in the SEM image of the NiAl–28Cr–6Mo alloy (Fig. 2b).

The densities of the alloys determined by Archimedes' principle are given in Table 2. The relative densities obtained by dividing the measured density values and the calculated theoretical density values give knowledge concerning the porosity level of the alloys. It was also observed that the relative densities of Mo-free alloy were higher in comparison to other alloy.

The microhardness values of the NiAl–34Cr and NiAl–28Cr–6Mo alloys are found to be 288 ± 18 $HV_{0.1}$ and 306 ± 14 $HV_{0.1}$, respectively. A slight increase in the hardness of the alloy was observed with the addition of molybdenum.

As is mentioned in the experimental procedure, the cyclic oxidation kinetics of the alloys was investigated at 800–1000°C for 168 h. The kinetics of oxidation of the alloys was determined as a function of time based on the weight change per unit area [6]:

$$\Delta W = \frac{(m_2 - m_1)}{A}, \quad (1)$$

where ΔW is the weight change per unit area (mg cm^2), m_1 is the initial weight (mg), m_2 is the weight after each cycle (mg), A is the total surface area of the alloy (cm^2). The correlation coefficients and equations concerned with weight change data are listed in Table 3.

The weight change per unit area of the alloys as a function of time is shown in Figs. 3a, 3b). The weight change per unit area of both alloys increased with increasing temperature. As oxidation time increased, the oxidation rate of the alloys decelerated and the weight changes of both alloys were the smallest in the last (final) 48 hours. The weight change was associated with the exfoliation of oxidation products formed on the surface, when the oxidation products had good adhesion to the substrate, the positive weight change occurred. In contrast, when the oxidation products exfoliated, the negative weight change was recorded [19]. When the oxidation temperature was elevated from 800 to 1000°C, the weight change of NiAl–34Cr alloy increased approximately 3 times, while that of NiAl–28Cr–6Mo alloy increased approximately 3.5 times. This increase in weight change shows that temperature has a significant effect on the oxidation behavior of alloys. During the initial stage of the oxidation test at 1000°C, a pronounced weight change was experienced by both samples. The reasons for this phenomenon can be attributed to two considerations. First one is that the diffusion rate of oxygen and metallic cations increases because of the elevation in temperature, and another one is that the alloy surfaces are fresh. After oxidation for 168 h, the overall weight change of the NiAl–34Cr and NiAl–28Cr–6Mo alloys were 21.25 and 19.86 mg cm^{-2}, respectively.

For all test temperatures the weight change of the Mo-containing alloy is less than that of the other alloy. Thus, it can be concluded that the addition of Mo has an effect which reduces the weight change of the alloy. Peng et al. [3] examined the isothermal oxidation behavior of various NiAl–(Cr,Mo) eutectic alloys at 900°C and found that the weight change of the at % NiAl–10Mo alloy decreased significantly around

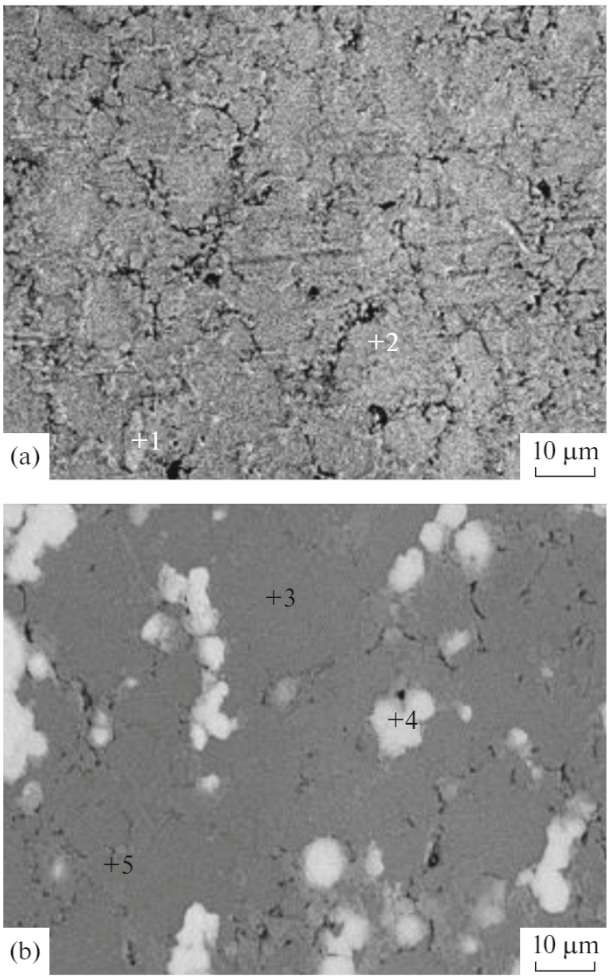

Fig. 2. SEM images of the microstructures of produced (a) NiAl–34Cr, (b) NiAl–28Cr–6Mo alloys.

Table 1. Chemical compositions of points shown in Fig. 2

Analysis Points	Element, at %			
	Ni	Al	Cr	Mo
1	4.7	4.9	90.4	–
2	58.2	35.9	5.9	–
3	42.7	54.0	2.2	1.1
4	32.5	30.4	26.3	10.8
5	20.0	16.8	58.8	4.4

Table 2. Density values of alloys produced by RS method

Alloys	Measured, g/cm^3	Theoretical, g/cm^3	Relative, %
NiAl–34Cr	5.68	5.79	98.10
NiAl–28Cr–6Mo	5.91	6.04	97.85

Table 3. Various equations determined by regression analysis of weight change data (Figs. 3a, 3b)

Alloy	800°C		900°C		1000°C	
	ΔW	R^2	ΔW	R^2	ΔW	R^2
NiAl–34Cr	$0.2315\ t^{0.6538}$	0.98	$2.0718\ t^{0.3782}$	0.99	$6.0712\ t^{0.2504}$	0.98
NiAl–28Cr–6Mo	$1.3827\ t^{0.280}$	0.97	$0.9178\ t^{0.5036}$	0.98	$4.4843\ t^{0.3056}$	0.94

1.1 h. The authors attributed this to the volatilization of MoO_3 above 700°C. A similar result was observed in the oxidation study of NiAl–20Mo (at %) alloy by Ray et al. [20].

No weight loss was observed in NiAl–28Cr–6Mo alloy related to the evaporation of MoO_3 at the beginning of oxidation in the weight change kinetics obtained in this study at 800–1000°C. We believe this is due to the low Mo content of the studied alloy compared to those reported. It should be noted that during the cyclic oxidation test, no scale spallation was observed for both alloys.

The data of weight change per unit area (ΔW) of the alloys versus oxidation time (t) have been analyzed to obtain the kinetic parameters such as oxidation rate constant (k_n) and oxidation rate exponent (n). A power law equation is used as follows [6]:

$$(\Delta W)^n = k_n t. \tag{2}$$

Taking the logarithm of Eq. (2) as follows we have:

$$\ln(\Delta W) = (1/n)\ln kn + (1/n)\ln t. \tag{3}$$

Thus, the values of n can be determined by analysis of the slope of the best fit line for a double logarithm plot of the weight change per unit surface area versus oxidation time. The oxidation rate exponent is based on the parameter $n = 1/R$, which is the reverse of the

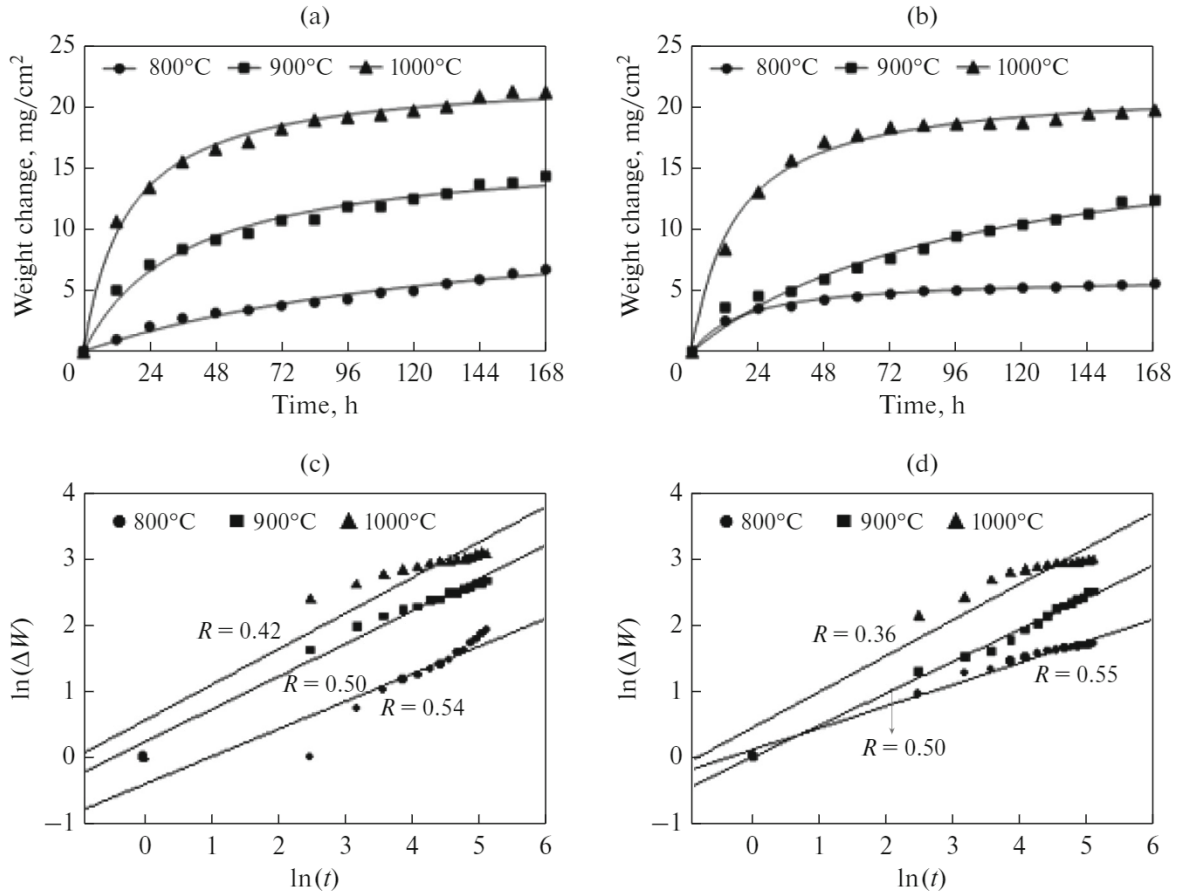

Fig. 3. Plots of weight change vs. oxidation time and ln (ΔW) vs. ln (t) for the oxidized alloys, (a, c) NiAl–34Cr, (b, d) NiAl–28Cr–6Mo.

Table 4. Calculated values of n and oxidation rate constants (k_n, $mg^n\ cm^{-2n}\ h^{-1}$) for the oxidized alloys at 800–1000°C

Alloy	800°C		900°C		1000°C	
	n	k_n	n	k_n	n	k_n
Ni–33Al–34Cr	2.38	0.5364	2	1.2129	1.85	1.407
Ni–33Al–28Cr–6Mo	2.77	0.7057	2	0.9445	1.81	1.2122

slope determined from the linear regression in Figs. 3c, 3d.

The relationship between the n value and the oxidation kinetics can be described as follows: $n = 1, 2, 3$ correspond to linear, parabolic, and cubic kinetics, respectively.

It can be said that the oxidation kinetics of the alloys at 800°C obeys a rate law intermediate between parabolic and cubic, while those of the alloys at 900 and 1000°C obey parabolic and nearly parabolic kinetics, respectively. After the determination of oxidation kinetics models for studied alloys, the values of oxidation rate constants (k_n) can be obtained from a linear regression fitting of $(\Delta W)^n$ against time. The corresponding rate exponents (n) and oxidation rate constants are presented in Table 4.

By considering the listed data in Table 4, the values of k_n decrease with the temperature decrease for the alloys. It is worth noting that a lower value of oxidation rate constant would mean a smaller rate of oxidation. On the base of k_n value, the oxidation resistance of NiAl–28Cr–6Mo alloy at 900 and 1000°C is higher than that of NiAl–34Cr alloy, but NiAl–28Cr–6Mo alloy exhibits lower oxidation resistance at 800°C as it follows cubic kinetics law. It was found that the k_n value of NiAl–28Cr–6Mo alloy decreased by 30% compared to the other alloy at 900°C where parabolic oxidation kinetics was observed. The parabolic rate kinetics is controlled by diffusion species involved in oxidation and, as oxidation time increases, the distance that the ions will diffuse to increases depending on the oxide scale thickness [6]. It was suggested that the addition of Cr has the effect of increasing the parabolic rate constant of NiAl alloys [3]. In addition, it was reported that the oxidation behavior of NiAl–Cr alloys is greatly affected by the oxides formed on the surface such as θ-Al_2O_3, α-Al_2O_3, and Cr_2O_3. Besides, influence of Cr addition on the oxidation resistance of NiAl–0.05Hf (at %) alloy was studied by Leyens et al. and they found that Cr element (up to 10 at %) has harmful effects on the oxidation behavior at 1100–1200°C [9]. The activation energy for oxidation can be estimated from Fig. 4 by considering that the relation between the oxidation rate constant and the temperature and can be expressed by an Arrhenius type equation: $k_n = k_0\exp(-Q/RT)$, where k_0 is the frequency factor, Q is the activation energy, R is the gas constant, and T is the temperature (K). Thus, the slope of the best-fit line in the Arrhenius plot corresponds to Q/R. The calculated activation energy values for NiAl–34Cr and NiAl–28Cr–6Mo alloys were 57 and 31 kJ mol^{-1}, respectively.

Figures 5a, 5b indicates the XRD patterns of the oxidized surfaces. According to XRD analysis results, oxide scales of both alloys consist of Cr_2O_3, α-Al_2O_3, NiO, and $NiAl_2O_4$ phases. In addition to these oxide phases, XRD patterns was found in extremely high-intensity matrix phases, which means that the oxide scale formed on the surface of the alloys is thin.

The reactions that may occur during the oxidation of the alloys examined in this study are listed in Table 5. It was reported that the $NiAl_2O_4$ spinel can exist in thermodynamic equilibrium with Al_2O_3, NiO and Ni in the ternary Ni–Al–O equilibrium at 1000°C [16]. The surface morphologies of the alloys after oxidation at 800–1000°C for 168 hours are shown in Fig. 6. The chemical compositions corresponding to the points are presented in Table 6. After oxidation of NiAl–34Cr alloy at 800°C, it was found that the surface consists of dark (marked as 1) and bright (marked as 2) phase areas. According to the EDS analysis results in Table 6, the chemical composition of the dark area corresponds to Al_2O_3 and that of the bright area corresponds to Cr_2O_3. Since the growth rate of Cr_2O_3 was larger than that of Al_2O_3 [21], the surface could not be rapidly covered by Al_2O_3, resulting in the formation of undulant morphology. In addition, Cr_2O_3 may play an

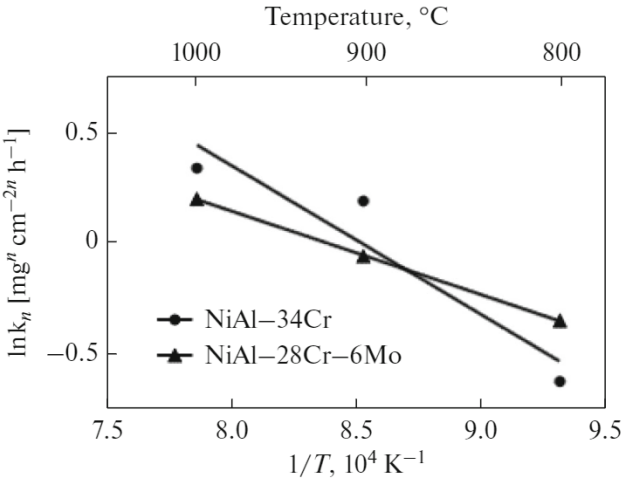

Fig. 4. Arrhenius plot of the logarithm of k_n at investigated temperatures vs. $1/T$.

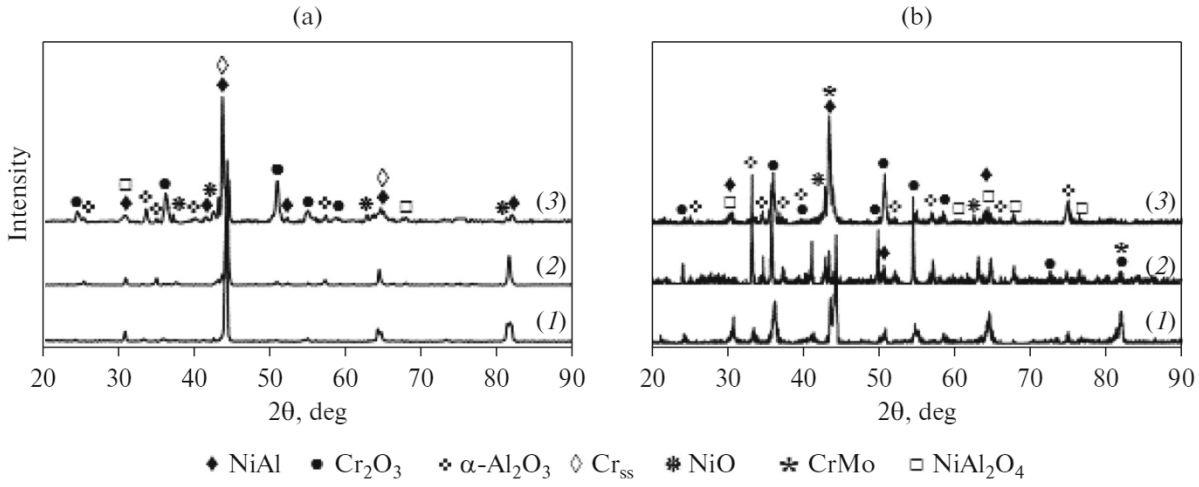

Fig. 5. XRD patterns of the oxidized alloys for 168 h (a) NiAl–34Cr, (b) NiAl–28Cr–6Mo ((*1*) 800, (*2*) 900, (*3*) 1000°C).

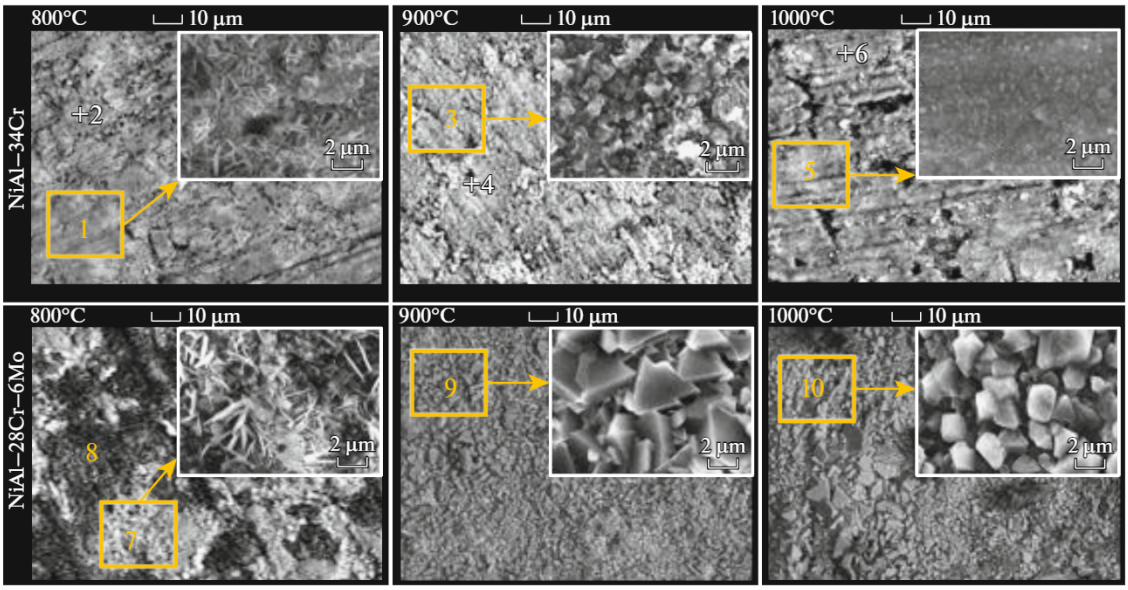

Fig. 6. SEM surface morphologies of oxidized alloys at 800–1000°C for 168 h.

important role against oxidation at lower temperature ($T < 1000$°C) but volatile CrO_3 is formed at a higher temperature.

The vaporization of CrO_3 changes depending on the oxidation temperature and time. The higher magnification of point 1 indicates that Al_2O_3 grains formed on the NiAl–34Cr alloy had rod-like morphology. When the oxidation temperature is elevated at 900°C, it was observed that the Al_2O_3 morphology formed at 800°C changed into a round shape. The chemical

Table 5. The values of Gibbs free energy for possible reactions (kJ/mol) (calculated by HSC Chemistry 6.0)

Reaction	ΔG°_{800}	ΔG°_{900}	ΔG°_{1000}
$4/3Al_{(s)} + O_{2(g)} = 2/3Al_2O_{3(s)}$	–891.14	–869.04	–847.01
$2/3Mo_{(s)} + O_{2(g)} = 2/3MoO_{3(s)}$	–317.20	–304.53	–292.16
$4/3Cr_{(s)} + O_{2(g)} = 2/3Cr_2O_{3(s)}$	–568.66	–551.99	–535.36
$Ni_{(s)} + 1/2O_{2(g)} = NiO(s)$	–142.21	–133.57	–124.97
$NiO_{(s)} + Al_2O_{3(s)} = NiAl_2O_{4(s)}$	–	–	–18.7
$MoO_3(s) + Ni + 1/2O_{2(g)} = NiMoO_4$	–129.02	–96.81	–63

Table 6. The chemical composition of points 1–10 shown in Fig. 6

Analysis points	Element, at %				
	Ni	Al	Cr	Mo	O
1	0.8	34.7	5.6	–	58.9
2	0.6	0.8	33.6	–	65
3	0.4	33.1	6.9	–	59.6
4	0.2	4.3	33.6	–	61.9
5	1.2	34.2	6.9	–	57.7
6	14.2	27.6	2.1	–	56.1
7	0.6	13.8	24.3	0.4	60.9
8	3.1	32.1	4.4	0.3	60.1
9	44.7	1.4	3.4	0.1	50.4
10	40.1	3.2	4.8	0.1	51.8

composition of the bright area (marked as 4) corresponds to Cr_2O_3 (Table 6). After 168 hours of exposure at 1000°C, the magnified SEM image of point 5 shows that there was an Al_2O_3 with a denser morphology. The Ni : Al ratio at point 6 is found to be about 1 : 2 in the EDS analysis results. This obtained result can be evidence of the formation of the $NiAl_2O_4$ phase, which is confirmed by XRD analysis. After 168 hours of oxidation at 800°C, the surface of the NiAl–28Cr–6Mo alloy consists mainly of gray (point 7) and dark (point 8) areas. As can be seen in the EDS analysis results, the gray phase region consists of an aluminum and chromium oxide mixture, while the dark region consists of aluminum oxide. From the high magnification SEM image of point 7, it can be seen that the oxide grains have a blade-like morphology. The surface morphology of the alloy after oxidation at 900 and 1000°C for 168 hours is quite different from that of the NiAl–34Cr alloy at the same temperature as it can be seen at Fig. 6. The alloy surface is entirely covered with polyhedron oxide grains. By considering the data in Table 6, it can be said that the formed oxide on the alloy was NiO. It is worth mentioning that the size of oxide grains increased with the increase of oxidation temperature.

CONCLUSIONS

In the present study, the cyclic oxidation behavior of NiAl–34Cr (at %) and NiAl–28Cr–6Mo alloys produced by RS method was studied at 800, 900, and 1000°C for 168 h. The following main conclusions can be drawn from this study:

(1) NiAl–34Cr and NiAl–28Cr–6Mo (at %) alloys consisted of NiAl + Cr and NiAl + CrMo phases, respectively.

(2) The values of micro hardness and relative density of the NiAl–34Cr and NiAl–28Cr–6Mo alloys are found to be 288 ± 18 $HV_{0.1}$ and 306 ± 14 $HV_{0.1}$, 98.10 and 97.85% respectively.

(3) NiAl–34Cr alloy approximately follows parabolic oxidation kinetics ($n = 2$) in the temperatures ranging from 800 to 1000°C, whereas NiAl–28Cr–6Mo alloy about follows parabolic oxidation kinetics ($n = 2$) at 900–1000°C. However, NiAl–28Cr–6Mo alloy nearly follows cubic oxidation kinetics ($n = 2.77$) at 800°C. The activation energy for NiAl–34Cr and NiAl–28Cr–6Mo alloys was 57 and 31 kJ mol^{-1}, respectively.

(4) Cr_2O_3, α-Al_2O_3, NiO, and $NiAl_2O_4$ phases were determined on the surfaces of oxidized alloys at 800–1000°C for 168 hours.

FUNDING

This research was performed within the framework of project 2017-01-08-041. We thank the Commission for Scientific Researcch Projects of Sakarya University for funding this project.

REFERENCES

1. K. S. Mohammed and H. T. Naeem, "Effect of milling parameters on the synthesis of Al-Ni intermetallic compound prepared by mechanical alloying," Phys. Met. Metallogr. **116**, No 9, 859–868 (2015).
2. A. S. Shchukin and A. E. Sytschev, "Peculiarities of a NiAl/Mo transition zone formed during self-propagating high-temperature synthesis," Phys. Met. Metallogr. **120**, No 9, 848–852 (2019).
3. J. Peng, X. Fang, Z. Qu, and J. Wang, "Isothermal oxidation behavior of NiAl and NiAl-(Cr,Mo) eutectic alloys," Corros Sci. **151**, 27–34 (2019).
4. H. Bei and E. P. George, "Microstructures and mechanical properties of a directionally solidified NiAl–Mo eutectic alloy," Acta Mater. **53**, 69–77 (2005).
5. P. Ferrandini, W. W. Batista, and R. Caram, "Influence of growth rate on the microstructure and mechanical behaviour of a NiAl–Mo eutectic alloy," J. Alloy Compd. **381**, 91–98 (2004).
6. Y. Garip and O. Ozdemir, "A study of the cycle oxidation behavior of the Cr/Mn/Mo alloyed Ti–48Al-based intermetallics prepared by ECAS," J. Alloy Compd. **818**, 152818 (2019).
7. Y. Garip and O. Ozdemir, "Comparative study of the oxidation and hot corrosion behaviors of TiAl–Cr intermetallic alloy produced by electric current activated sintering," J. Alloy Compd. **780**, 364–377 (2019).
8. T. Yener, A. Erdoğan, M. S. Gök, and S. Zeytin, "Nb and B effect on mechanical properties of Ti–Al based intermetallic materials," Vacuum **169**, 108867 (2019).
9. C. Leyens, B. A. Pint, and I. G. Wright, "Effect of composition on the oxidation and hot corrosion resistance of NiAl doped with precious metals," Surf. Coat. Technol. **133–134**, 15–22 (2000).
10. P. Y. Hou and K. Priimak, "Interfacial segregation, pore formation, and scale adhesion on NiAl alloys," Oxid. Met. **63**, 113–130 (2000).

11. M. W. Finnis, A. Y. Lozovoi, and A. Alavi, "The oxidation of NiAl: What Can We Learn from Ab Initio Calculations?," Annu. Rev. Mater. Res. **35**, 167–207 (2000).
12. Z. Zhang, L. Li, and J. C. Yang, "γ-Al2O3 thin film formation via oxidation of β-NiAl(110)," Acta Mater. **59**, 5905–5916 (2011).
13. Zhao, C., Zhou, Y., Zou, Z., Luo, L., Zhao, X., and Guo, F., "Effect of alloyed Lu, Hf and Cr on the oxidation and spallation behavior of NiAl," Corros. Sci. **126**, 334–343 (2017).
14. L. Wang, D. Li, J. Chang, H. Guo, S. Gong, and H. Xu, "Isothermal oxidation behavior of dysprosium/S–doped β-NiAl alloys at 1200°C," J. Mater. Sci. Technol. **30**, 229–233 (2014).
15. G. Zhang, H. Zhang, and J. Guo, "Improvement of cyclic oxidation resistance of a NiAl-based alloy modified by Dy," Surf. Coat. Technol. **201**, 2270–2275 (2006).
16. D. Prajitno, B. Gleeson, and D. J. Young, "The cyclic oxidation behaviour of α-Cr + β-NiAl alloys with and without trace Zr addition," Corros. Sci. **39**, No. 4, 639–654 (1997).
17. B.Tang, D. A. Cogswell, G. Xu, S. Milenkovic, and Y. Cui, "The formation mechanism of eutectic microstructures in NiAl–Cr composites," Phys. Chem. Chem. Phys. **18**, 19773–19786 (2016).
18. G. K. Dey, "Physical metallurgy of nickel aluminides," Sadhana **28**, 247–262 (2003).
19. K. Zhang, T. Zhang, X. Zhang, and L. Song, "Corrosion resistance and interfacial morphologies of a high Nb-containing TiAl alloy with and without thermal barrier coatings in molten salts," Corros. Sci. **156**, 139–146 (2019).
20. P. K. Ray, M. Akinc, and M.J. Kramer, "Formation of multilayered scale during the oxidation of NiAl–Mo alloy," Appl. Surf. Sci. **301**, 107–111 (2014).
21. Z.-S. Wang, Y. Xie, J.-T. Guo, L.-Z. Zhou, Z.-Q. Hu, G.-Y. Zhang, and Z.-G. Chen, "High temperature oxidation behavior of directionally solidified NiAl–31Cr–2.9Mo–0.1Hf–0.05Ho eutectic alloy," Trans. Nonferrous Met. Soc. China **22**, 1582–1587 (2012).